Eric Ou
Department of Mechanical Engineering,
The University of Texas at Austin,
Austin, TX 78712
e-mail: eric.ou@utexas.edu

Xun Li
Department of Mechanical Engineering and
Materials Science,
University of Pittsburgh,
Pittsburgh, PA 15261
e-mail: xul34@pitt.edu

Sangyeop Lee
Department of Mechanical Engineering and
Materials Science,
Department of Physics and Astronomy,
University of Pittsburgh,
Pittsburgh, PA 15261
e-mail: sylee@pitt.edu

Kenji Watanabe
Research Center for Functional Materials,
National Institute of Materials Science,
1-1 Namiki,
Tsukuba 305-0044, Japan
e-mail: WATANABE.Kenji.AML@nims.go.jp

Takashi Taniguchi
Research Center for Functional Materials,
National Institute of Materials Science,
1-1 Namiki,
Tsukuba 305-0044, Japan
e-mail: TANIGUCHI.Takashi@nims.go.jp

Li Shi[1]
Department of Mechanical Engineering,
The University of Texas at Austin,
Austin, TX 78712
e-mail: lishi@mail.utexas.edu

Four-Probe Measurement of Thermal Transport in Suspended Few-Layer Graphene With Polymer Residue

The presence of unknown thermal contact thermal resistance has limited prior two-probe thermal transport measurements of suspended graphene samples. Here, we report four-probe thermal transport measurements of suspended seven-layer graphene. By isolating the thermal contact resistance, we are able to attribute the observed reduced thermal conductivity primarily to polymeric residue on the sample instead of the contact thermal resistance, which resulted in ambiguity in the prior experimental studies of the effect of polymer reside. The extrinsic scattering rate due to the polymer residue is extracted from the measurement results based on a solution of the Peierls-Boltzmann phonon transport equation. [DOI: 10.1115/1.4043167]

Introduction

Graphitic materials are among the best-known thermal conductors. The basal-plane thermal conductivity of graphite and its derivatives, including graphene and carbon nanotubes, rivals the record high value of diamond. Although the high thermal conductivity of both diamond and graphitic materials can be generally described by Slack's high thermal conductivity criteria based on strongly bonded light elements [1], there are intriguing unanswered questions on the microscopic mechanisms behind the distinctly high thermal conductivity of graphitic materials. One unusual feature in the atomic vibration spectrum of graphitic materials is the presence of an out-of-plane bending or flexural modes for which the frequency increases quadratically with increasing wavevector. Compared to the in-plane polarized modes, these low-frequency flexural modes dominate the specific heat and make an important contribution to the high basal-plane thermal conductivity of graphene according to the first principles calculation [2]. Moreover, the crystal momentum is conserved during the scattering among a large population of small-wavevector flexural phonon modes, similar to intermolecular scattering in terms of momentum conservation. Recent first-principle calculations have suggested that the normal scattering processes dominate over momentum nonconserving umklapp phonon–phonon scattering processes in both suspended graphene, graphite and single wall carbon nanotubes, even near room temperatures [3–6]. Consequently, phonon transport in graphene and graphite can exhibit hydrodynamic transport features similar to molecular flows, including unique size and temperature dependences that cannot be explained by either diffusive transport described by Fourier's law or ballistic phonon transport theory captured by the Landauer-Büttiker formalism [7].

The presence of these unusual nondiffusive, ballistic, or hydrodynamic features in the intrinsic phonon transport process can have a practical impact on the dependence of the apparent thermal conductivity of the graphitic materials on the size, shape, temperature, and interface interaction. Therefore, experimental investigation of these nondiffusive behaviors has become an area of intense research over the past two decades. However, there are a number of challenges for experimental observation of the nondiffusive phonon transport behaviors in graphitic materials. While sensitive thermal transport measurements have been devised to observe the temperature dependence and size dependence in the thermal conductivity of carbon nanotubes and graphene [8–13], an important

[1]Corresponding author.
Contributed by the Heat Transfer Division of ASME for publication in the Journal of Heat Transfer. Manuscript received October 2, 2018; final manuscript received March 7, 2019; published online April 17, 2019. Assoc. Editor: Evelyn Wang.

limitation is the inability of these methods to separate the extrinsic thermal contact resistance from the intrinsic thermal resistance of the sample [14–16]. This limitation can complicate the interpretation of the experimental results. While a two-probe thermal transport measurement has suggested that the measured thermal conductivity of suspended graphene increases with length due to nondiffusive phonon transport [11], it is found that the experimental data can also be attributed to contact thermal resistance that was not measured directly in the two-probe thermal measurement [17]. In addition, while prior two-probe thermal measurements have concluded that the interaction between the graphene and an amorphous support [12] or polymer residue layer [13] can suppress the graphene thermal conductivity, it has been questioned whether the suppression was actually due to contact thermal resistance that was not measured in the two-probe measurements [18].

In this paper, we report a four-probe thermal transport measurement of both the extrinsic thermal contact resistance and the intrinsic thermal conductivity of a suspended seven-layer graphene sample in order to determine both the contact thermal resistance and the intrinsic thermal conductivity of the graphene sample. The experimental results clearly reveal that polymer residue, instead of the contact thermal resistance, is the main cause of the observed suppressed thermal conductivity and diffusive phonon transport behaviors. Theoretical analysis of the measurement results further allows us to extract the phonon scattering rate by polymer residue.

Experimental Methods

The few-layer graphene (FLG) sample was exfoliated from a synthetic graphite powder source grown by a high-temperature, high-pressure process onto silicon wafer pieces with a 290 nm thick silicon oxide layer for optical contrast. After patterning the FLG with electron beam lithography and oxygen plasma etching, four palladium (Pd) lines were deposited on the patterned graphene in a lift-off process. The FLG sample and the Pd lines were transferred onto the microfabricated device with the use of a polymethylmethacrylate (PMMA) carrier film. After the PMMA was removed in acetone, the sample was dried in a critical point dryer. Clamping the graphene sample between the top Pd lines and the underlying suspended metal lines helps to prevent the suspended graphene sample from being washed away or folded during the acetone removal process. The device was then measured in a cryostat under high vacuum.

The optical micrograph in Fig. 1(*a*) and the scanning electron microscopy image in Fig. 1(*b*) show the FLG sample assembled on the four-probe thermal measurement device, which consisted of four suspended Pd thermometer lines deposited on top of patterned silicon nitride (SiN_x) beams. The sample segment suspended between the two middle lines, for which we can find the thermal conductance using the thermal circuit shown in Fig. 1(*c*), is 3.8 μm wide and 13.0 μm long. Based on atomic force microscopy measurements of the sample on the silicon wafer prior to the patterning process, the sample is seven layers thick, as shown in Fig. 2.

Figure 1(*c*) shows a thermal circuit of the sample on the four-probe thermal measurement device. The measurement is performed by resistively heating a single metal thermometer line while simultaneously measuring the electrical resistances of all thermometer lines as seen in Fig. 3. A floating voltage source is used to provide the heating current to the metal line without an electrical current flowing into the graphene sample to the other thermometer lines. A 50 kΩ precision resistor is connected between the voltage source and the heating line and serves to limit the heating current. The electrical resistance of the heating line is obtained from the four-terminal current (I)–voltage (V) data that are measured with the use of low-noise current and voltage preamplifiers, respectively, similar to the procedure described in a prior publication [19]. The electrical resistances of the other

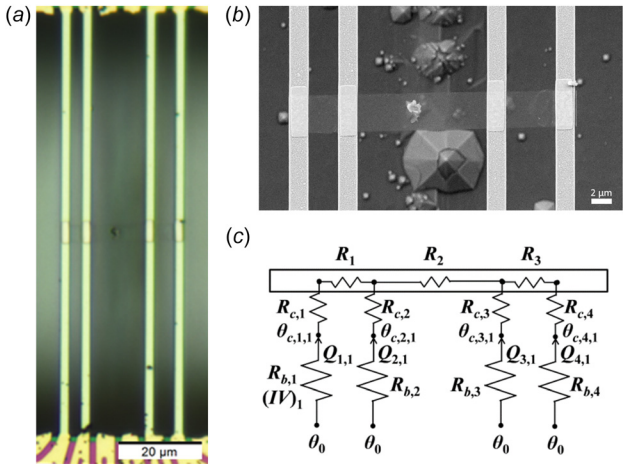

Fig. 1 (*a*) Optical and (*b*) scanning electron micrographs of a 3.8 μm wide, seven-layer thick patterned FLG sample assembled across four suspended Pd/SiN_x beams, each of which acts as a resistance thermometer (RT). Additional Pd pads were deposited on top of the FLG sample to clamp the graphene sample onto the thermometer lines. The black dots left on the sample and metal lines are polymeric dirt particles. (*c*) Thermal resistance circuit of the measurement device when the first thermometer line is Joule heated with power $(IV)_1$. $R_{b,j}$ is the thermal resistance of the jth RT beam. $R_{c,j}$ represents the thermal contact resistance between the sample and the jth RT. R_1, R_2, and R_3 represent the intrinsic thermal resistances of the three suspended sample segments. $\theta_{c,j,i}$ is the jth RT temperature rise at the contact point with the sample when the ith line is heated. θ_0 is the temperature rise at the point where the suspended RT lines terminate into the bulk substrate. $Q_{j,i}$ is the heat flow from the jth line to the sample when the ith line is heated.

thermometer lines are measured individually with the use of a small 1 μA sinusoidal excitation current and a lock-in amplifier to measure the voltage drop along the thermometer line. This process is repeated until each metal line has been electrically heated. By measuring the electrical resistance of the thermometer lines at different temperatures with a low bias current, shown in Fig. 4, we obtain the temperature coefficient of resistance and use it to convert the measured change in electrical resistance during Joule heating to the average temperature rise in each thermometer line. Based on the parabolic and linear temperature profiles for the heating line and the thermometer lines, respectively, the contact point temperature rise between line j and the sample for heated

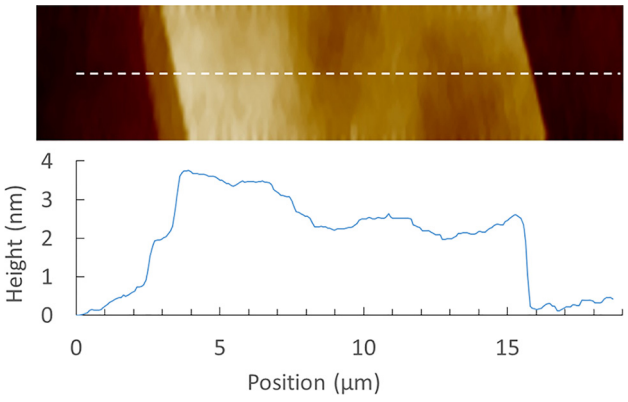

Fig. 2 Atomic force microscope scan of the seven-layer graphene sample before patterning. The thickness of the sample was determined by averaging the step height measured at multiple points on the right edge of the scan.

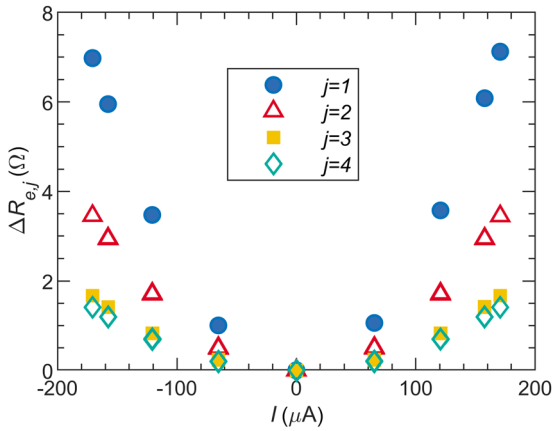

Fig. 3 Measured electrical resistance change of the thermometer lines as a function of the heating current through the first thermometer line

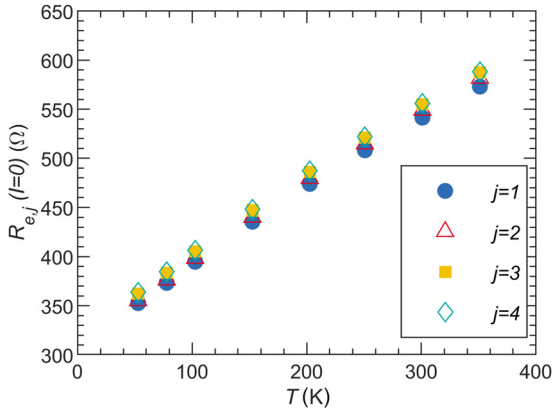

Fig. 4 Measured electrical resistances of the four thermometer lines at a low bias current as a function of the stage temperature

line i with a Joule heating rate $(IV)_i$, $\theta_{c,j,i}$, can be obtained from the measured average temperature rise, as shown in the analytical solutions reported in recent works [20,21].

The sixteen $\theta_{c,j,i}/(IV)_i$ data with both i and j ranging from 1 to 4 can allow us to obtain the thermal resistance of the four thermometer lines ($R_{b,j}$), the intrinsic thermal resistance of the sample (R_2), and the contact resistances ($R_{c,2}$ and $R_{c,3}$) between the sample and the thermometer lines 2 and 3, as well as the combined intrinsic and contact thermal resistance, $R_1 + R_{c,1}$ and $R_3 + R_{c,4}$, of the two end segments of the sample [21]. Here, R_2 can be separated from $R_{c,2}$ and $R_{c,3}$ because the heat flow through the middle sample segment differs from that through each of the two middle contacts. In comparison, the heat flow through an end segment is the same as that through the corresponding end contact, so that the intrinsic thermal resistance of the end segment cannot be separated from the end contact thermal resistance.

Figure 5 shows the measured thermal resistances at different temperatures. The thermal resistances of the thermometer lines are comparable to the intrinsic thermal resistance of the middle suspended segment. This condition, which is close to optimum for this comparative thermal measurement, improves the signal to noise ratio in the difference of the measured temperature responses of the two middle thermometer lines. In addition, the electronic thermal conductance of each metal thermometer line

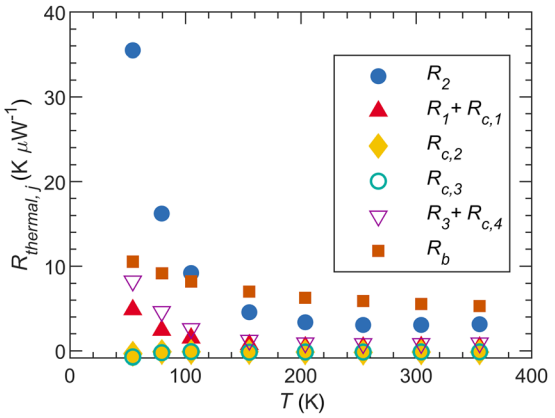

Fig. 5 Measured thermal resistances of the sample and the average thermal resistance of the thermometer lines. The random uncertainty of the values does not exceed the marker size.

can be obtained from the measured electrical resistance ($R_{e,j}$) and the Wiedemann–Franz law, so that the lattice thermal conductivity of the SiN_x beam under the metal line can be obtained as

$$\kappa_{SiN} = \frac{L}{2A}\left(\frac{1}{R_{b,j}} - \frac{4L_0T}{R_{e,j}}\right) \tag{1}$$

where L and A are the total length and the cross section of each suspended SiN_x beam, respectively, L_0 is the Lorentz number, and T is the absolute temperature. The obtained room-temperature κ_{SiN_x} range from 3.6 to 3.8 W m^{-1} K^{-1}, which agrees with the literature report for similar low-stress SiN_x [22].

The directly measured contact thermal resistances ($R_{c,2}$ and $R_{c,3}$) of the transferred sample are negligible compared to the intrinsic thermal resistance (R_2) of the middle-suspended segment of the sample. This finding reveals that the four Pd clamps that were transferred together with the FLG were effective in reducing the contact thermal resistance. The ability of separating the contact thermal resistance and directly obtaining the intrinsic thermal resistance here has allowed us to eliminate an important source of error in the measured thermal transport property.

Results and Discussion

The obtained thermal conductivity increases with increasing temperature to reach 500 ± 21 W m^{-1} K^{-1} at room temperature as shown in Fig. 6. At room temperature, the thermal conductivity is less than a quarter of the highest basal-plane value reported for bulk graphite [23]. In addition, the observed temperature dependence differs from that for high-quality graphite for which the thermal conductivity peaks at a low temperature near 100 K and decreases with increasing temperature above 100 K due to an increase of intrinsic Umklapp phonon–phonon scattering processes. In comparison, the observed peak temperature is close to 300 K for the FLG sample. This shift of the peak temperature dependence reveals the dominance of extrinsic phonon scattering processes compared to intrinsic phonon–phonon scattering.

Extrinsic scattering mechanisms include boundary scattering at the two side edges and the two end contacts of the suspended middle segment of the few-layer graphene sample. To investigate the impact of side edge and end contact scattering, we have used a first principles calculation to find the temperature-dependent thermal conductivity of a suspended single-layer graphene (SLG) sample with a similar width and length. The effects of finite sample size and aspect ratio were included by solving the Peierls-Boltzmann transport equation of phonons in both reciprocal and real space domains [24]. Both the temperature dependence and the magnitude of the calculation results are much closer to the

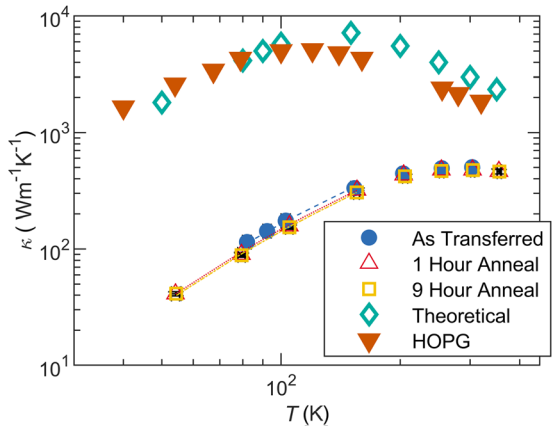

Fig. 6 Measured thermal conductivity of the FLG as a function of temperature for the as-transferred (circles), 1 h annealed (unfilled up triangles), and 9 h annealed sample (squares). Shown for comparison is the highest basal-plane thermal conductivity reported for bulk highly oriented pyrolytic graphite (down triangles) in Touloukian et al. [23], and the theoretical thermal conductivity (diamonds) of a defect-free single layer graphene sample with the same lateral dimension as the measured FLG. The lines are the fitting of the experimental data by using the calculated phonon dispersion of seven-layer graphene and a frequency-dependent scattering rate.

highest reported thermal conductivity data of high-quality graphite than to the measurement results of the few-layer graphene sample, as shown in Fig. 6. According to a previous theoretical study [25], in addition, the difference in the thermal conductivity of FLG and SLG of a similar dimension is much smaller than that between the measured FLG sample and the calculated SLG. These results reveal that side edge scattering and end scattering are not the cause of the reduced thermal conductivity of the seven-layer graphene sample.

Other extrinsic scattering mechanisms are point defects and grain boundaries that can be present in the synthetic graphite sample and scattering by the polymer residue left on the top surface of the transferred graphene sample. The presence of polymer residue is clearly revealed in the optical image that shows a dark particle on top of the center region of the middle-suspended segment of the graphene. In addition to this particle, the apparent brightness contrast showing the graphene sample in the optical image is

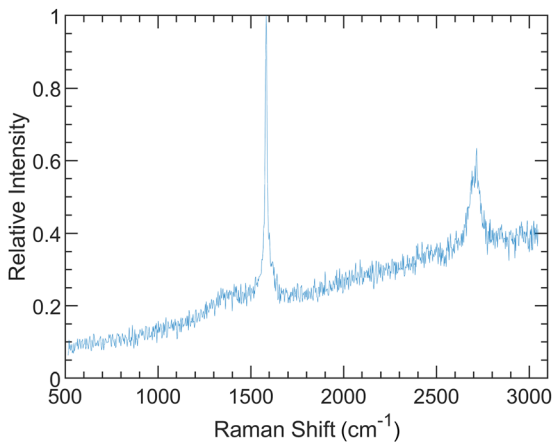

Fig. 7 Raman spectrum of the middle suspended segment of the sample. The background slope is indicative of the presence of polymer residue.

largely caused by the presence of a residual polymer layer on the suspended graphene sample. As an attempt to reduce the polymer residue, the sample was annealed at 350 °C in flowing argon and hydrogen and subsequently re-measured after 1 h of annealing and again after an additional 8 h of annealing. However, the annealing did not yield apparent changes in either the optical contrast of the FLG sample or the measured thermal conductivity. As shown in Fig. 7, the Raman spectra measured on the FLG sample upon the annealing do not show a D peak that is caused by defects but reveal a background slope that is indicative of the presence of polymer residue. Thus, the suppressed thermal conductivity cannot be attributed to point defect scattering of phonons.

In comparison, the polymer residue layer increases the mass of the suspended graphene membrane, impedes both the out-of-plane and in-plane vibration of the graphene atoms according to a theoretical study [26], and suppresses the measured basal plane thermal conductivity contributions from both the in-plane and the out-of-plane polarized phonon modes [12,13]. Based on the calculated phonon dispersion of a seven-layer graphene sample, we determine the rate of combined extrinsic defect scattering and intrinsic phonon–phonon scattering that can fit the theoretical thermal conductivity with the measurement results. The extracted relaxation time is found to increase with increasing phonon frequency as $\tau^{-1} \propto \omega^{\alpha}$, where α is 0.162, 0.135, and 0.137 for the measured results for the as-transferred, 1 h annealed, and 9 h annealed sample, respectively. The increasing τ^{-1} with phonon frequency indicates that the intrinsic phonon–phonon scattering is not negligible compared to the extrinsic scattering by polymeric residue, given that the former increases with phonon frequency while the latter decreases with phonon frequency [12].

Conclusion

The four-probe measurement has obtained both the extrinsic thermal contact resistance and the intrinsic thermal conductivity of the seven-layer graphene sample exfoliated from synthetic graphite. As the contact resistance error has been eliminated in this four-probe measurement, the result has allowed us to unambiguously conclude that the observed suppressed thermal conductivity is not due to this measurement error. Our analysis shows that the suppressed thermal conductivity and the increasing peak temperature are not caused by edge or end scattering that would cause ballistic phonon transport. Instead, scattering by the polymer residue left on the top surface plays an important role and result in diffusive phonon transport in the suspended few-layer graphene sample. In order to observe nondiffusive thermal transport features including ballistic and hydrodynamic phonon transport that has been predicted to be important in high-quality graphite and graphene [3,4], it is necessary to first measure a high thermal conductivity that decreases with increasing temperature for temperatures higher than about 100 K, where Umklapp phonon–phonon scattering is expected to be dominant. In conjunction with the four-probe thermal transport measurement method reported here, further progress in polymer-free assembly of high-quality graphene samples may lead to eventual observation of intrinsic nondiffusive phonon transport phenomena that have been pursued in experiments over the past two decades [17].

Acknowledgment

We would like to thank Dr. Jaehyun Kim and Brandon Smith for their helpful discussions. We acknowledge use of Texas Nanofabrication Facilities supported by the NSF NNCI Award 1542159. This work was supported in part by NSF Awards 1707080 and 1705756 on Hydrodynamic Thermal Transport in Graphitic Materials. The simulation was performed using Linux clusters of the XSEDE (TG-CTS180043) and the University of Pittsburgh Center for Research Computing.

Funding Data

- NSF NNCI (Award No. 1542159; Funder ID: 10.13039/501100008982).
- NSF (Award Nos. 1707080 and 1705756; Funder ID: 10.13039/501100008982).

Nomenclature

A = area (m^2)
I = electrical current (A)
L = length (m)
L_0 = Lorentz number ($W\Omega/K^2$)
R = thermal resistance (K/W)
R_e = electrical resistance (Ω)
T = temperature (K)
V = voltage (V)

Greek Symbols

θ = temperature rise (K)
κ = thermal conductivity (W/m K)
τ = relaxation time (s)
ω = phonon frequency (rad/s)

Subscripts

b = beam
c = contact
e = electrical
i = heated line index
j = sensing line index

References

[1] Slack, G. A., 1973, "Nonmetallic Crystals With High Thermal Conductivity," J. Phys. Chem. Solids, **34**(2), pp. 321–335.
[2] Lindsay, L., Broido, D. A., and Mingo, N., 2010, "Flexural Phonons and Thermal Transport in Graphene," Phys. Rev. B, **82**(11), p. 115427.
[3] Ding, Z., Zhou, J., Song, B., Chiloyan, V., Li, M., Liu, T.-H., and Chen, G., 2018, "Phonon Hydrodynamic Heat Conduction and Knudsen Minimum in Graphite," Nano Lett., **18**(1), pp. 638–649.
[4] Lee, S., Broido, D., Esfarjani, K., and Chen, G., 2015, "Hydrodynamic Phonon Transport in Suspended Graphene," Nat. Commun., **6**(1), p. 6290.
[5] Cepellotti, A., Fugallo, G., Paulatto, L., Lazzeri, M., Mauri, F., and Marzari, N., 2015, "Phonon Hydrodynamics in Two-Dimensional Materials," Nat. Commun., **6**(1), p. 6400.
[6] Lee, S., and Lindsay, L., 2017, "Hydrodynamic Phonon Drift and Second Sound in a (20,20) Single-Wall Carbon Nanotube," Phys. Rev. B, **95**(18), p. 184304.
[7] Chen, G., 2005, *Nanoscale Energy Transfer and Conversion*, Oxford University Press, New York.
[8] Kim, P., Shi, L., Majumdar, A., and McEuen, P. L., 2001, "Thermal Transport Measurements of Individual Multiwalled Nanotubes," Phys. Rev. Lett., **87**(21), p. 215502.
[9] Shi, L., Li, D., Yu, C., Jang, W., Kim, D., Yao, Z., Kim, P., and Majumdar, A., 2003, "Measuring Thermal and Thermoelectric Properties of One-Dimensional Nanostructures Using a Microfabricated Device," ASME J. Heat Transfer, **125**(5), p. 881.
[10] Pettes, M. T., and Shi, L., 2009, "Thermal and Structural Characterizations of Individual Single-, Double-, and Multi-Walled Carbon Nanotubes," Adv. Funct. Mater., **19**(24), pp. 3918–3925.
[11] Xu, X., Pereira, L. F. C., Wang, Y., Wu, J., Zhang, K., Zhao, X., Bae, S., Tinh Bui, C., Xie, R., Thong, J. T. L., Hong, B. H., Loh, K. P., Donadio, D., Li, B., and Özyilmaz, B., 2014, "Length-Dependent Thermal Conductivity in Suspended Single-Layer Graphene," Nat. Commun., **5**(1), p. 3689.
[12] Seol, J. H., Jo, I., Moore, A. L., Lindsay, L., Aitken, Z. H., Pettes, M. T., Li, X., Yao, Z., Huang, R., Broido, D., Mingo, N., Ruoff, R. S., and Shi, L., 2010, "Two-Dimensional Phonon Transport in Supported Graphene," Science, **328**(5975), pp. 213–216.
[13] Pettes, M. T., Jo, I., Yao, Z., and Shi, L., 2011, "Influence of Polymeric Residue on the Thermal Conductivity of Suspended Bilayer Graphene," Nano Lett., **11**(3), pp. 1195–1200.
[14] Wang, Z., Xie, R., Bui, C. T., Liu, D., Ni, X., Li, B., and Thong, J. T. L. L., 2011, "Thermal Transport in Suspended and Supported Few-Layer Graphene," Nano Lett., **11**(1), pp. 113–118.
[15] Wang, H., Hu, S., Takahashi, K., Zhang, X., Takamatsu, H., and Chen, J., 2017, "Experimental Study of Thermal Rectification in Suspended Monolayer Graphene," Nat. Commun., **8**, p. 15843.
[16] Wang, J., Zhu, L., Chen, J., Li, B., and Thong, J. T. L., 2013, "Suppressing Thermal Conductivity of Suspended Tri-Layer Graphene by Gold Deposition," Adv. Mater., **25**(47), pp. 6884–6888.
[17] Jo, I., Pettes, M. T., Lindsay, L., Ou, E., Weathers, A., Moore, A. L., Yao, Z., and Shi, L., 2015, "Reexamination of Basal Plane Thermal Conductivity of Suspended Graphene Samples Measured by Electro-Thermal Micro-Bridge Methods," AIP Adv., **5**(5), p. 053206.
[18] Yu, C., and Zhang, G., 2013, "The Underestimated Thermal Conductivity of Graphene in Thermal-Bridge Measurement: A Computational Study," J. Appl. Phys., **113**(21), p. 214304.
[19] Seol, J. H., Moore, A. L., Shi, L., Jo, I., and Yao, Z., 2011, "Thermal Conductivity Measurement of Graphene Exfoliated on Silicon Dioxide," ASME J. Heat Transfer, **133**(2), p. 022403.
[20] Kim, J., Ou, E., Sellan, D. P., and Shi, L., 2015, "A Four-Probe Thermal Transport Measurement Method for Nanostructures," Rev. Sci. Instrum., **86**(4), p. 044901.
[21] Smith, B., Vermeersch, B., Carrete, J., Ou, E., Kim, J., Mingo, N., Akinwande, D., and Shi, L., 2017, "Temperature and Thickness Dependences of the Anisotropic in-Plane Thermal Conductivity of Black Phosphorus," Adv. Mater., **29**(5), p. 1603756.
[22] Huxtable, S. T., Cahill, D. G., and Phinney, L. M., 2004, "Thermal Contact Conductance of Adhered Microcantilevers," J. Appl. Phys., **95**(4), pp. 2102–2108.
[23] Touloukian, Y. S., Powell, R. W., Ho, C. Y., and Klemens, P. G., 1971, *Thermophysical Properties of Matter: Thermal Conductivity of Nonmetallic Solids*, Ifi/Plenum, New York.
[24] Li, X., and Lee, S., 2018, "Role of Hydrodynamic Viscosity on Phonon Transport in Suspended Graphene," Phys. Rev. B, **97**(9), p. 94309.
[25] Lindsay, L., Broido, D. A., and Mingo, N., 2011, "Flexural Phonons and Thermal Transport in Multilayer Graphene and Graphite," Phys. Rev. B, **83**, p. 235428.
[26] Qiu, B., and Ruan, X., 2012, "Reduction of Spectral Phonon Relaxation Times From Suspended to Supported Graphene," Appl. Phys. Lett., **100**(19), p. 193101.